CHEMISTRY OF BASALTS FROM LEG 45 OF THE DEEP SEA DRILLING PROJECT

by

J. M. Rhodes[1], D. P. Blanchard[2], M. A. Dungan[3], K. V. Rodgers[1] and J. C. Brannon[1]

[1]Lockheed Electronics Company, Inc., Houston, Texas
[2]NASA, Johnson Space Center, Houston, Texas
[3]NRC Research Associate, Johnson Space Center, Houston, Texas

INTRODUCTION

A total of 764 m of volcanic basement was sampled during Leg 45 at Sites 395 and 396, the vast majority of which consisted of basaltic pillow lavas, thin flows, and more massive cooling units. This paper is concerned with the major and trace element chemistry of these basalts. A companion paper by Dungan et al., (this volume) discusses the petrography, mineral chemistry and one-atmosphere melting experiments for the same suite of samples. Emphasis will be placed on samples recovered at Site 395 from Holes 395 and 395A. Data for samples from Site 396, Hole 396, are included for completeness, but will be reported on in detail, together with data on samples from Hole 396B in the Leg 46 Initial Report.

Major and trace element analyses for 59 basalt samples from holes 395 and 395A are given in Table 1; analyses for 8 samples from Hole 396 are given in Table 2. In these tables, the samples are listed in order of increasing depth within the basement, reported to the nearest meter. Also indicated in Tables 1 and 2 are the major magmatic compositional units, which were identified initially on the basis of shipboard x-ray fluorescence analyses, and modified slightly in the light of the recent data. Within these two tables, the oxidation ratio (O.R.) is given as Fe_2O_3/(Total iron as FeO). The atomic ratio Mg/(Mg+Fe) has been calculated after adjustment for the oxidation state of iron such that the ratio Fe^{3+}/(Total iron as Fe^{2+}) is 0.1 (Bass, 1971). For convenience the atomic Mg/(Mg+Fe) ratio is designated the Mg'-value in Tables 1 and 2 and throughout the paper. The same convention for handling the oxidation state of iron has been used in the CIPW norm calculations that are referred to in the text and illustrated in Fig. 5.

Table 3 presents additional trace element data on 26 of the samples selected from Table 1, on the basis of petrography and major element chemistry.

The major element data were obtained by x-ray fluorescence analysis (XRF) on fused glass discs, prepared by fusing the sample with a lanthanum-bearing lithium borate fusion mixture (Norrish and HUtton, 1969). FeO was determined titrimetrically using the modified cold acid digestion method of Wilson (Maxwell, 1968), and Fe_2O_3 was obtained by difference from the XRF total iron value. Na_2O was obtained on a separate 20-30 mg aliquant by instrumental neutron activation analysis (INAA). Total water content was measured coulometrically using a DuPont moisture analyzer, in which the sample is fused with a lead oxide flux.

The trace elements (Rb, Sr, Y, Zr, Nb, Ni) were determined by XRF analysis on pressed powder pellets. Corrections were made for non-linear backgrounds, tube contamination, and inter-element interferences (Norrish and Chappell, 1967). Corrections for matrix effects were based on a modification of the Compton scattering method (Reynolds, 1967), using the Ag-Compton peak. Additional trace element data (Table 3) (La, Ce, Sm, Eu, Tb, Yb, Lu, Hf, Cr, Sc, Ni) were obtained by INAA following the methods of Jacobs et al., (1976).

BASALT CHEMISTRY

All the basalts recovered from Holes 395, 395A and 396 are olivine and hypersthene normative, containing between 1.8 and 14.2 percent of normative olivine, and plotting in the olivine tholeiite field of the basalt tetrahedron (Yoder and

Tilley, 1962). Alkali basalts and transitional tholeiites are conspicuously absent, as also are quartz tholeiites. They have the overall compositional characteristics typical of mid-ocean ridge tholeiites, as is evidenced by their relatively constant SiO_2 concentrations and low TiO_2 abundances, together with low total alkali content and K_2O/Na_2O ratios (e.g., Engel et al., 1965; Melson et al., 1976). K_2O abundances are characteristically low in the majority of samples (<0.2%) and, where comparative data is available, do not differ significantly from the K_2O content of basaltic glass from the same samples. A few samples have higher K_2O contents not related to basalt type presumably the result of sea water alteration, although this is not always correlated with total water content or the oxidation ratio.

The minor and trace element abundances are, similarly, within the range of typical mid-ocean ridge tholeiites (Kay et al., 1970; Schilling,1971; Pearce and Cann, 1973; Hart, 1976; Bryan et al., 1976; Erlank and Kable, 1976). This is illustrated by the chondrite-normalized rare-earth patterns, which range between 13 and 24 times chondritic abundances for Sm, and which display the light rare-earth depletion typical of "normal" or type I ocean ridge basalts (Bryan et al., 1976). Mg'-values in these rocks are variable, ranging from about 0.57 to 0.67 (Fig. 1), which is within the range prevalent for mid-ccean ridge basalts but is lower than the values found in the most primitive basalts identified to date (Frey et al., 1974; Bryan and Moore, 1976; Rhodes et al., in prep.). These values, together with low Ni concentrations, moderately high magmaphile element abundances, and the presence of multiple phenocryst phases (Dungan et al., this volume), are taken as evidence that these basalts have all undergone a substantial differentiation history.

The majority of samples selcted for analysis were relatively fresh, with total water contents usually less than 2 percent and with oxidation ratios mostly below 0.4. Consequently it is unlikely that the major or trace element chemistry of these samples will have been significantly modified by sea water alteration. The mobile elements K, Rb, and S are notable exceptions. The effects of alteration on sulfur are particularly pronounced, and there is a marked inverse correlation between the oxidation ratio and the sulfur content (Fig. 2). It would appear from this relationship that unaltered samples should contain about 0.14 percent sulfur, a value somewhat larger than that proposed by Moore and Fabbi (1971) as typical for unaltered basalts recovered from deep water.

Two broad basalt types, differing fundamentally in both petrography and whole-rock chemistry, are prevalent at Site 395. These are, respectively, the aphyric and phyric basalts. The aphric basalts lack megascopic phenocrysts, but contain microphenocrysts of olivine or olivine and plagioclase, whereas the phyric basalts contain abundant (10-30%) plagioclase phenocrysts, together with phenocrysts of olivine, rarer Cr-diopside plus minor chromian spinel. The aphyric basalts are the most abundant, comprising about 59 percent of the cored interval.

Chemically, the phyric basalts are distinguished from the aphyric basalts by higher Al_2O_3 (16.5-19.2%) and CaO(11.5-12.8%) concentrations, and by lower SiO_2, FeO and MgO concentrations (Figs. 3,4). These differences are reflected in

higher normative plagioclase contents and in lower Ab/(Ab+An) ratios in the phyric basalts. Although both total iron and MgO are lower in the phyric basalts, Mg'-values tend to be higher, an indication that they are more "primitive" than the aphyric basalts (Figs. 1,4). TiO_2, and most other minor and magmaphile trace element abundances are markedly lower in the phyric basalts (Fig. 1). This difference extends also to the glassy rims of the phyric basalts, and is therefore not simply a consequence of plagioclase dilution. Strontium, on the other hand, is higher in the phyric basalts, both in absolute terms and with respect to other magmaphile elements. Consequently, Sr/Zr ratios are distinctly different in the two basalt types, varying widely in the phyric basalts (1.55-2.46) in contrast to the lower, essentially constant values (1.02-1.18) found in the aphyric basalts.

Figure 5 illustrates the normative olivine, plagioclase and pyroxene relationships for these basalts, relative to the inferred olivine-plagioclase cotectic of Shido et al., (1971). All the aphyric basalts plot in the olivine tholeiite field, within a tightly controlled elongate group sub-parallel to the inferred cotectic. In contrast, the phyric basalts plot predominantly within the plagioclase tholeiite field and are widely scattered. Those phyric basalts plotting close to the inferred cotectic, or just within the olivine tholeiite field, have the lowest Al_2O_3 contents. Presumably, they contain fewer plagioclase phenocrysts than the majority of samples, and may be closer to melt compositions. As might be expected from these relationships in one atmosphere melting experiment on a typical phyric basalt (#138), plagioclase is the first phase to crystalize, followed by olivine, whereas in a typical aphyric basalt (#122), olivine is the liquidus phase, followed by plagioclase (Dungan et al., this volume).

Initial studies, based on shipboard x-ray fluorescence analyses, recognized within the two major basalt types ten compositionally distinct magmatic units. These were, in order of increasing depth below the sediment-basement interface, A1, A2, P1, P2, P3, P4, P5, A3, A4, P4, A4, and A5, where A denotes aphyric and P phyric basalt respectively.

Our data essentially confirms these subdivisions, subject to minor revisions in the light of the more recent and comprehensive data. Average values, calculated from the data in Table 1, are given in Table 4. In order of increasing depth within Hole 395A, the following compositional units can be identified.

Aphyric unit-A2 (106-173m) — This is the uppermost aphyric unit, occurring in the upper 29m of Hole 395, as well as in 395A. It consists of a thick sequence of chemically homogeneous, rapidly chilled pillow basalts, and has a characteristic variolitic texture containing microphenocrysts of olivine. This basalt type is distinguished from the other aphyric basalts principally on the basis of higher iron concentrations (10.6-11.1%) and by slightly lower abundances of strontium (Table 4). The compositional variation is small, and is commensurate with minor (<5%) olivine fractionation.

In the initial shipboard studies the magmatic unit A1 was based on a single sample (11-1-103-108) near the top of the basement in Hole 395. It was more iron-rich than underlying members of the A2 basalts. In order to locate the A1-A2 boundary we have analyzed basalts immediately above and below this sample, and find that they have typical A2 compositions (Table 1 #109,110). From this we conclude that unit A1 is not a distinct magmatic unit, and that the iron-rich sample analyzed during shipboard studies is a more evolved variant of the A2 basalt type.

Phyric unit-P2 (173-201m) — This unit occurs at the top of the thick 181m sequence of phyric basalts that were cored in Hole 395A, and also occurs in the bottom 10m of hole 395. In Hole 395A, almost the whole of this unit is composed of a single thick (25m), massive cooling unit. With the exception of the lowermost sample in the cooling unit (Table 1, #130), the P2 basalts are uniform in composition, and are more evolved than the other phyric basalts. This is reflected in lower Mg'-values and higher abundances of TiO_2 and other magmaphile elements (Fig. 1). The lowermost sample in the cooling unit is higher in Al_2O_3, has a higher Mg'-value and has correspondingly lower abundances of magmaphile elements. In many respects it resembles other, more "primitive" phyric basalts lower in the stratigraphic sequence. We attribute this difference either to preferential accumulation of plagioclase and olivine phenocrysts at the base of the cooling unit, or to upward migration of interstitial magma due to filter pressing.

Phyric unit-P3 (201-260m) — This unit is distinguished from the other phyric units by lower TiO_2 and magmaphile element abundances (Figs. 1,7). Strontium is also low in this unit (110-119 ppm) relative to all the other phyric basalts. The plagioclase-olivine phyric basalt associated with the brecciated serpentinized peridotite zone in Hole 395 is also low in strontium (Table 1, #115), and tends to be lower in magmaphile elements than most other phyric basalts. In many respects, it closely resembles the P3 basalt type in Hole 395A, and may simply be fragments of this basalt type incorporated into the breccia zone, rather than a separate magmatic unit (P1) as was suggested by the shipboard studies.

Phyric units-P4, P5 (260-356m) — Initial shipboard anlyses indicated that these two basalt types are essentially similar in bulk chemistry, but differ in strontium content. Additional analyses reported here (Table 1) show that both units exhibit a wide range in strontium values, with P4 varying between 122 and 165 ppm, and P5 between 132 and 175 ppm. Consequently, we believe that the initial distinction between these two basalt types is no longer tenable.

As a group these basalts are highly variable both in Al_2O_3 content, which varies from 16.1 to 19.1 percent, and in Mg'-values that range between 0.59 and 0.67. Much of this variability must be attributed to localized variation in plagioclase and olivine phenocryst content.

Deeper in the section (608-629m) there is a massive (21m) cooling unit that is chemically equivalent to the P4-P5 phyric basalts. This is believed to be a sill that intruded underlying aphyric basalts penecontemporanesouly with extrusion of the P4-P5 basalts.

Aphyric unit-A3 (356-570m) — This exceptionally thick sequence of compositionally uniform pillow basalts is more evolved than the other aphyric units. These basalts are multiply saturated with microphenocrysts of both olivine and plagioclase (Dungan et al., this volume), and plot towards the low temperature end of the inferred cotectic in Fig. 5. Although the Mg'-values compare closely with those of the A2 basalts (e.g., 0.59-0.61), they are distinctly lower in both FeO and MgO (Fig. 4). and on the basis of Fig. 7 in Roeder and Emslie (1970), can be inferred to have lower liquidus temperatures. In keeping with their evolved nature, these basalts have the highest lithophile element abundances, and are

characterized by a more distinct Eu anomaly than is observed for the other aphyric basalts. The unit as a whole exhibits little compositional variation, and there are no obvious fractionation trends.

At the sediment-basement interface in Hole 395A is a rubble zone containing fragments of aphyric basalt, serpentinized peridotite, and gabbro (cores 4 and 5). Two of these basalts are indistinguishable from the A3 basalts (Table 1, # 117,118), suggesting that this basalt type is exposed at the surface of the basement within close proximity to the drill site.

Aphyric unit-A4 (570-608 and 629-657) — This unit is intruded by a 21m sill compositionally equivalent to the P4-P5 phyric basalts. There is no appreciable difference in chemistry between the basalts above the sill (Table 1, #155-160) and those beneath (Table 1, #161-168). All are aphyric basalts containing olivine microphenocrysts. They are both texturally and chemically similar to the A2 basalts, but can be distinguished from the latter by a tendency towards higher normative olivine contents (Fig. 5), higher Mg'-values (0.60-0.63), and lower total iron concentrations for a given value of MgO (Fig. 4). TiO_2, Sr and the magmaphile element abundances are essentially idential with the A2 basalts.

DISCUSSION

The chondrite-normalized rare-earth abundances for the Leg 45 samples (Fig. 6) show them to be "normal" LIL element-depleted basalts. They are light-rare earth depleted, with La/Sm and La/Yb ratios less than 1.0 (Table 4), similar to the Type I basalts of Bryan et al., (1976). The Nb content of these basalts is low, resulting in high Zr/Nb ratios (mean = 58) similar to those observed in other LIL element depleted basalts (Pearce and Cann, 1973; Erlank and Kable 1976; Rhodes et al., 1976), and considerably higher than the Zr/Nb ratios (<10) of oceanic islands and "anomalous" Type II basalts sampled on the Mid-Atlantic Ridge at 45°N and in the FAMOUS area (Erlank and Kable, 1976; Rhodes et al., unpublished data). Two $^{87}Sr/^{86}Sr$ values of 0.70276±10 and 0.70280±8, obtained for samples 117 and 153 respectively, are also characteristic of "normal", Type I LIL element-depleted basalts (Hart, 1976).

Inspection of Figs. 6,7 and Table 4 shows that most magmaphile element ratios are very similar for the various basalt types, and do not differ substantially between the phyric and aphyric basalts. An obvious exception is the ratio of strontium to other magmaphile elements. This is illustrated by the Sr/Zr ratio, which is constant in the aphyric basalts where Sr behaves as a magmaphile element, but is both distinctly different and highly variable in the phyric basalts where plagioclase influence is prevalent. Since many magmaphile element ratios and the characteristic REE patterns are not substantially changed by fractional crystallization involving the observed phenocryst phases, olivine and plagioclase, (Kay et al., 1970; Schilling 1971; Frey et al., 1974; Schilling, 1975) we deduce

that these ratios reflect the characteristics of the mantle source region, and that all of the various basalt types were derived from an essentially similar and homogeneous LIL-element depleted mantle source. Similar ratios are observed in basalts from Hole 396 (Table 2) and 396B (Dungan et al., Leg 46 initial report), implying a widespread and homogeneous mantle source for basaltic volcanism along this section of the Mid-Atlantic Ridge. This contrasts markedly with the wide variations in magmaphile element ratios found in Leg 37 basalts, both within and between holes (Blanchard et al., 1976), and the consequent necessity to postulate a complex and heterogeneous mantle source for the basalts in that region.

Although these basalts appear ultimately to have been derived by partial melting of a common source, all are evolved and have undergone moderate amounts of differentiation. Evidence of this is provided by the low Mg'-values (0.57-0.67), low Ni concentrations (<190 ppm), moderate magmaphile element abundances (e.g., TiO_2 — 1.0-1.7%), and the presence of multiple phenocryst phases in all but the A2 and A4 basalts. Since the compositional variation within the individual basalt groups is small, and there are no clearly defined internal fractionation trends, we suggest that magma compositions were established by differentiation within shallow magma chambers, followed by episodic eruption onto the sea floor, with little or no fractionation at the surface or enroute to the surface.

There can be little doubt that the compositions of the glassy and variolitic aphyric basalts are close to those of magmatic liquids. The compositions of the phyric basalts are more enigmatic. Several lines of evidence indicate that these

rocks are far removed from liquid compositions:

a) Compilations of basaltic glass compositions (Melson et al., 1976) indicate that magmatic liquids with more than 17 percent Al_2O_3 are extremely rare. Similarly, the glassy selvages on the phyric basalts (unpublished data) are much lower in Al_2O_3 and not substantially different from the aphyric basalts (Fig. 3).

b) The wide scatter of compositions in the normative olivine-plagioclase-pyroxene diagram (Fig. 5) is suggestive of plagioclase and olivine addition to liquids close to the inferred olivine-plagioclase cotectic. Plagioclase addition trends are also evident in several other variation diagrams (e.g., Figs. 3,4).

c) Dungan et al., (this volume) present experimental, textural and compositional evidence indicating that many of the plagioclase and olivine phenocrysts are too anorthitic or forsteritic to have crystallized from melts having the compositions of the phyric basalts, but derive instead from more "primitive" basalts.

From this evidence, we think that the phyric basalts have a mixed heritage, resulting from mixing of consanguineous "primitive" and evolved magmas and their attendant phenocrysts. If this interpretation is correct, the higher Mg'-values, normative An/(Ab+An) ratios, and lower magmaphile element abundances of the phyric basalts relative to the aphyric ones is due in part to the addition of up to 20 percent plagioclase and 5 percent olivine phenocrysts. The glassy rims on phyric basalt pillows probably provide the most reliable of the melt compositions. They have Mg'-values comparable to those of the more evolved aphyric basalts (<0.60), but are distinguished from them by lower TiO_2 values (Fig. 1) and by higher CaO/Al_2O_3 ratios. Thus, the phyric basalts are not simply related to any of the aphyric basalts types by processes of plagioclase and olivine accumulation.

An understanding of the relationships between the various phyric basalt units is also frustrated by the uncertainty concerning melt compositions. In terms of increasing magmaphile element abundances, the basalt types are ranked as follows, P3, P4-5, P2. This is not simply a function of decreasing plagioclase and olivine accumulation, but reflects a fundamental property of each of the basalt types. However, the increase in magmaphile element abundances from P3 to P2 is too large, and varied, to be accounted for simply by crystal fractionation of the dominant phenocryst phases, plagioclase and olivine, and cannot readily be reconciled with the absence of systematic changes in major element chemistry. We attribute these differences in the magmaphile element abundances in the phyric basalts to discrete magma types, containing varying proportions of admixed plagioclase, olivine, and rarer clinopyroxene phenocrysts.

The relationships between the three aphyric basalt units are less complicated. The A2 and A4 basalts are broadly similar in major and trace element chemistry, and both contain only olivine as the microphenocryst phase. The A2 basalts are higher in total iron and tend to have lower Mg'-values than the majority of the A4 basalts (Fig. 4). Consequently, these two basalt types cannot be related by olivine fractionation, the only observed phenocryst phase, and the liquidus phase in equilibrium melting experiments (Dungan et al., this volume). The A3 basalts contain microphenocrysts of both olivine and plagioclase and are more evolved than the stratigraphically lower A4 basalts, from which they may have been derived by olivine fractionation. However, the magmaphile element abundances are at variance with this interpretation. Some elements, such as Sr, Y and Sc

are increased in the A3 basalts relative to the A4 basalts, commensurate with the 5 percent olivine and plagioclase fractionation required by the major element data. The differences in other elements (e.g., Ti, Zr, La, Sm, Yb) are, however, too large to be the result of such a small amount of fractionation. Furthermore, the amounts of fractionation estimated from the reciprocal of the ratio of magmaphile elements in the A3 to the A4 basalts (Anderson and Greenland, 1969) is not constant for the different elements, and varies from as little as 4 percent for Sr, to as much as 20 percent for Sm. Clearly, these magma types are not related directly by crystal fractionation processes.

CONCLUSION

Thus we have, at the Leg 45 site, several discrete magma types, both phyric and aphyric, that are not related directly by crystal fractionation, but which appear to have been derived from a common mantle source. The prevailing interpretation of such relationships is that each basalt type represents an evolved derivative of more "primitive" basaltic magmas that resulted from varying amounts of melting of a common mantle source. The evidence, presented here of magma mixing in the phyric basalts suggests that such a model may be unduly simple. We suggest instead that magma mixing of consanguineous evolved and "primitive" basalts, together with their attendant phenocrysts, may go a long way towards explaining many of the characteristics of the basalts. A subsequent publication documenting the role of magma mixing in these and other ocean floor basalts is in preparation.

REFERENCES

Anderson A.T. and Greenland L.P. (1969) Phosphorus fractionation diagram as a quantitative indicator of crystallization differentiation of basaltic liquids. Geochim. Cosmochim. Acta 33, 493-505.

Bass M.N. (1971) Variable abyssal basalt populations and their relation to sea-floor spreading rates. Earth Planet. Sci. Lett. 11, 18-22.

Blanchard D.P., Rhodes J.M., Dungan M.A., Rodgers K.V., Donaldson C.H., Brannon J.C., Jacobs J.W. and Gibson E.K. (1976) The chemistry and petrology of basalts from Leg 37 of the Deep Sea Drilling Project. J. Geophys. Res., 81, 4231-4246.

Bryan W.B. and Moore J.G. (1976) Compositional variations of young basalts in the Mid-Atlantic Ridge rift valley near lat. 46°49'N. Bull. Geol. Soc. Amer., 88, 556-570.

Bryan W.B., Thompson G., Frey F.A., and Dickey J.J. (1976) Inferred settings and differentiation in basalts from the Deep Sea Drilling Project. J. Geophys. Res., 81, 4285-4304.

Dungan M.A., Long P.E. and Rhodes J.M. (1977) The petrography, mineral chemistry and one-atmosphere phase relations of basalts from Site 395 - Leg 45 DSDP. (This volume).

Engel A.E., Engel C.G. and Havens R.G. (1965) Chemical characteristics of oceanic basalts and the upper mantle. Bull. Geol. Soc. Amer., 76, 719-734.

Erlank A. J. and Kable E.J.D. (1976) The significant of incompatible elements in mid-Atlantic ridge basalts from 45°N with particular reference to Zr/Nb. Contrib. Mineral. Petrol., 54, 281-291.

Frey F.A., Bryan W.B. and Thompson G. (1974) Atlantic ocean floor: Geochemistry and petrology of basalts from Legs 2 and 3 of the Deep Sea Drilling Project. Jour. Geophys. Research 79, 5507-5527.

Hart S.R. (1976) LIL-element geochemistry, Leg 34 basalts, in Initial Reports of the Deep Sea Drilling Project, Leg 34, pp. 283-288, U.S. Government Printing Office, Washington, D.C.

Jacobs J.W., Korotev R.L., Blanchard D.P. and Haskin L.A. (1976) A well tested procedure for instrumental neutron activation analysis of silicate rocks and minerals. J. Radioanal. Chem. (in press)

Kay R., Hubbard N.J. and Gast P.W. (1970) Chemical characteristics and origin of oceanic ridge volcanic rocks. J. Geophys. Res., 75, 1585-1613.

Maxwell J.A. (1968) Rock and Mineral Analysis. Interscience.

Melson W.G., Vallier T.L., Wright T.L., Byerly G. and Nelen J. (1976) Chemical diversity of abyssal volcanic glass erupted along Pacific, Atlantic, and Indian ocean sea-floor spreading centers, in The Geophysics of the Pacific ocean basin and its margin, pp. 351-367. American Geophysical Union, Washington, D.C.

Moore J.G. and Fabbi B.P. (1971) An estimate of the juvenile sulfur content of basalt. Contrib. Mineral. Petrol., 33, 118-127.

Norrish K. and Chappell B.W. (1967) X-ray fluorescence spectrography. In Physical Methods in Determinative Mineralogy (editor J. Zussman), pp. 161-214, Academic Press.

Norrish K. and Hutton J.T. (1969) An accurate X-ray spectrographic method for the analysis of a wide range of geological samples. Geochim. Cosmochim. Acta 33, 431-453.

Pearce J.A. and Cann J.R. (1973) Tectonic setting of basic volcanic rocks determined using trace element analyses. Earth Planet. Sci. Lett., 19, 290-300.

Reynolds R.C. (1967) Estimation of mass absorption coefficients by Compton scattering: Improvements and extensions of the method. Am. Mineral., 48, 1133-1143.

Rhodes J.M., Blanchard D.P., Rodgers K.V., Jacobs J.W. and Brannon J.C. (1976) Petrology anc chemistry of basalts from the Nazca Plate: Part 2 - major and trace element chemistry, in Initial Reports of the Deep Sea Drilling Project, Leg 34, pp. 239-244. U.S. Government Printing Office, Washington, D.C.

Roeder P.L. and Emslie P.F. (1970) Olivine-liquid equilibrium. Contr. Mineral. and Petrol. 29, 275-289.

Schilling J.G. (1971) Sea-floor evolution: Rare-earth evidence. Phil. Trans. Roy. Soc. London, Ser. A. 268, 663-706.

Schilling J.G. (1975) Rare earth variations across 'normal segments' of the Reykjanes Ridge, 60°-53°N, mid-Atlantic ridge, 29°5, and East Pacific rise 2°-19°S, and evidence on the composition of the underlying low velocity layer. J. Geophys. Res. 80, 1459-1473.

Shido F.A., Miyashiro A. and Ewing M. (1971) Crystallization of abyssal tholeiites. Contrib. Mineral. Petrol., 31, 251-266.

Yoder H.S. and Tilley C.E. (1972) Origin of basalt magmas: an experimental study of natural and synthetic rock systems. J. Petrol. 3, 342-532.

Figure Captions

Fig. 1 TiO_2 versus Mg'-value for DSDP Leg 45 basalts. The field for abyssal volcanic glass compositions is taken from the data of Melson et al., (1976).

Fig. 2 The relationship of sulfur content to oxidation ratio (O.R.) in DSDP Leg 45 basalts. The juvenile sulfur content of the basalts is inferred to have been greater than 0.14 percent.

Fig. 3 Al_2O_3 versus MgO for DSDP Leg 45 basalts. The olivine and plagioclase control lines are for illustrative purposes only. They are not intended as lines of "best fit", or to imply that the basalts are related simply by olivine and plagioclase fractionation.

Fig. 4 MgO-FeO relationships for DSDP Leg 45 basalts. The dashed lines indicate Mg'-values from 0.5 to 0.7.

Fig. 5 Normative olivine-plagioclase-pyroxene relationships in DSDP Leg 45 basalts. The classification and inferred olivine-plagioclase cotectic is from Shido et al., (1971).

Fig. 6 Chondrite-normalized abundances in DSDP Leg 45 basalts.

Fig. 7 Lanthanum-Samarium and Zirconium-Yttrium relationships in DSDP Leg 45 basalts. The lines shown are for constant La/Sm and Zr/Y ratios.

NASA-S-77-11448

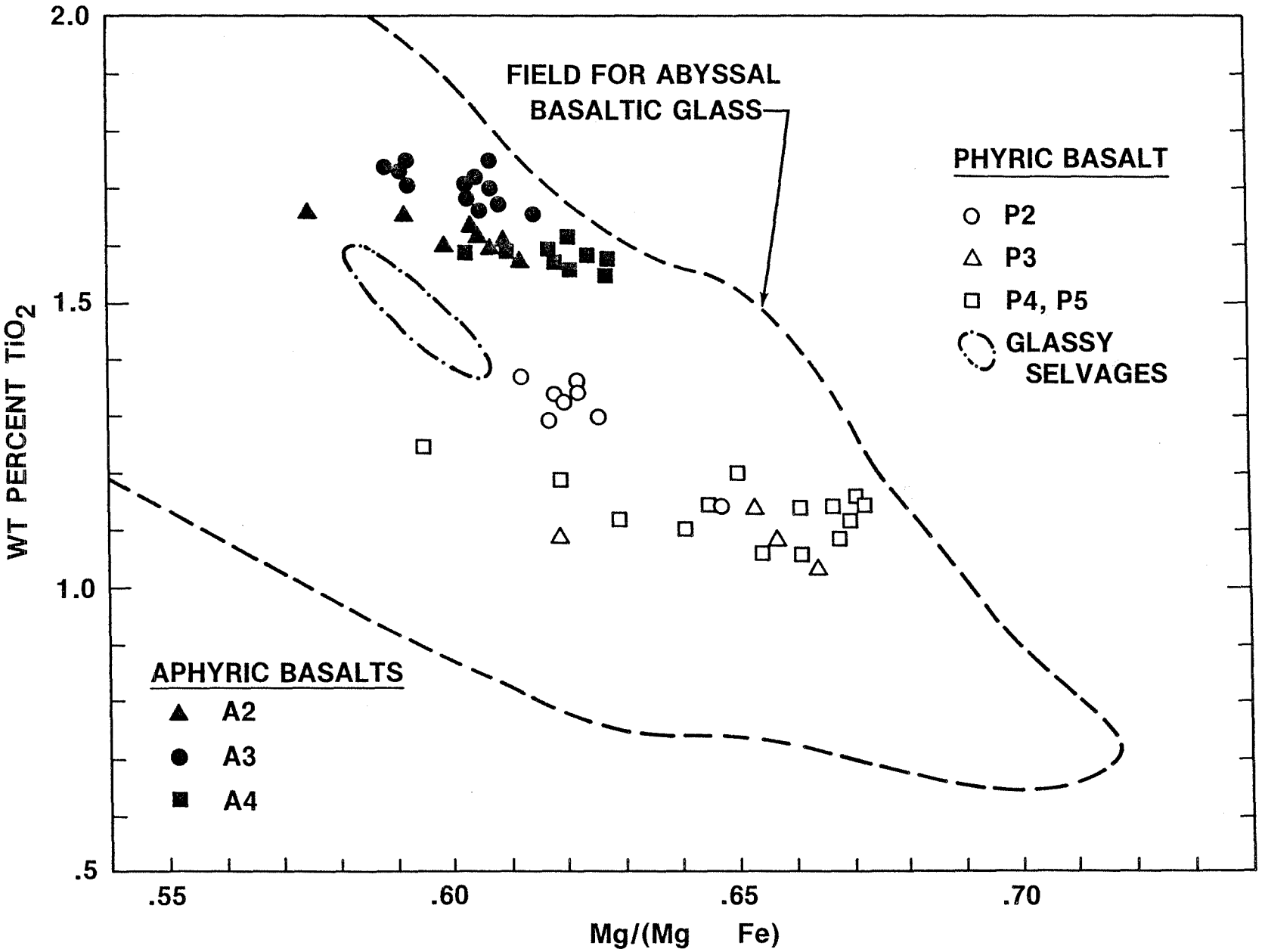

NASA-S-77-11446

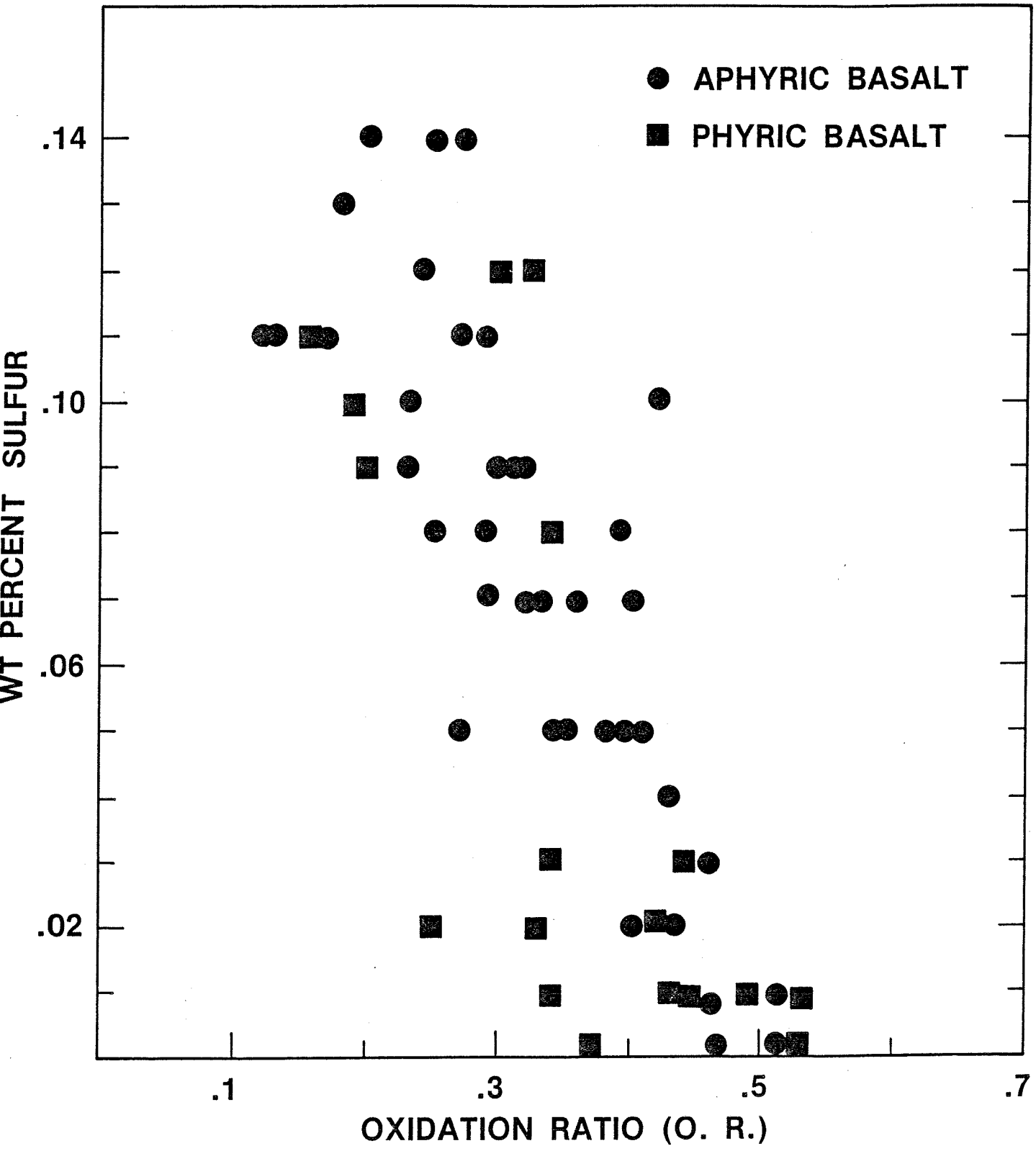

NASA-S-77-11451

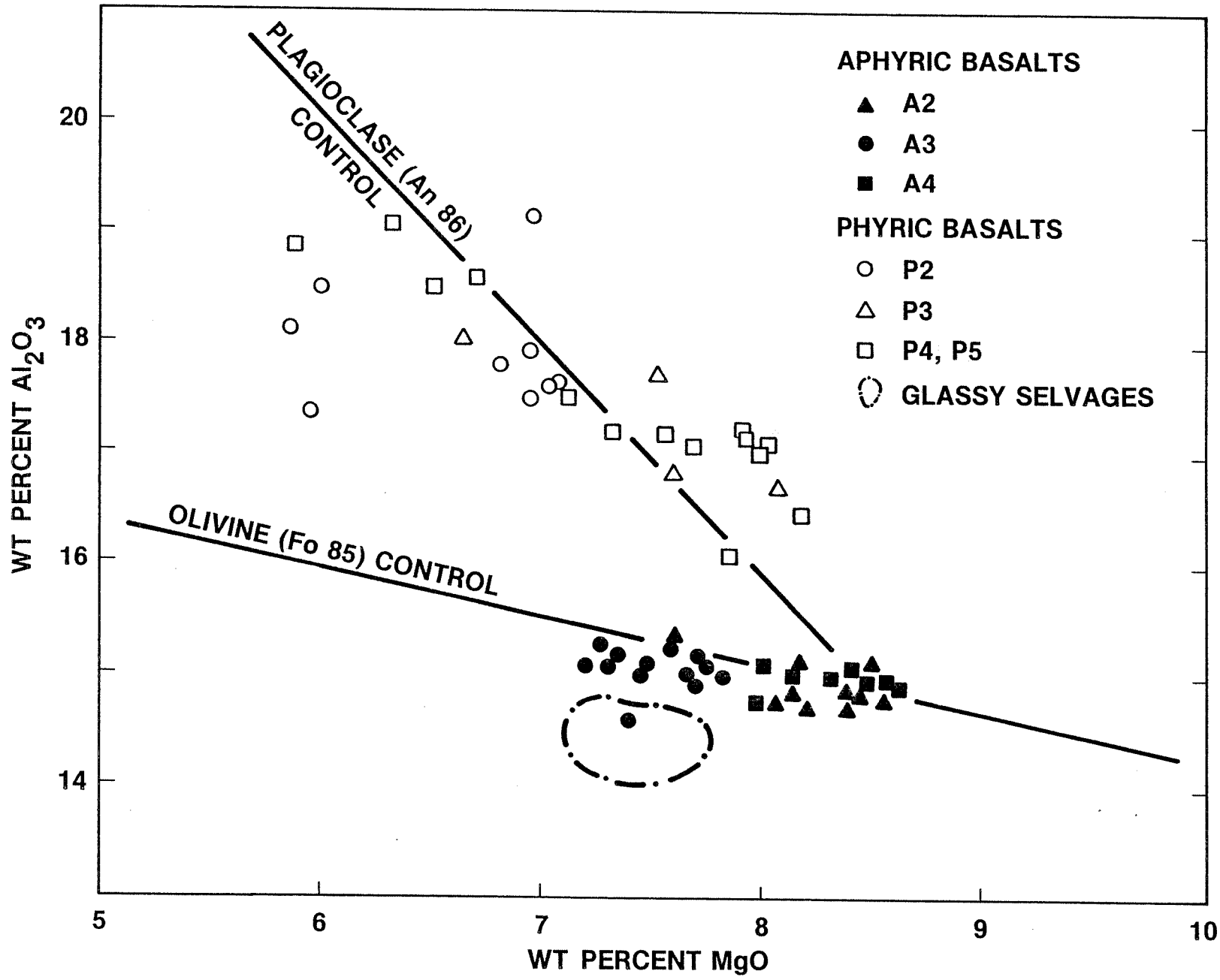

NASA-S-77-11450

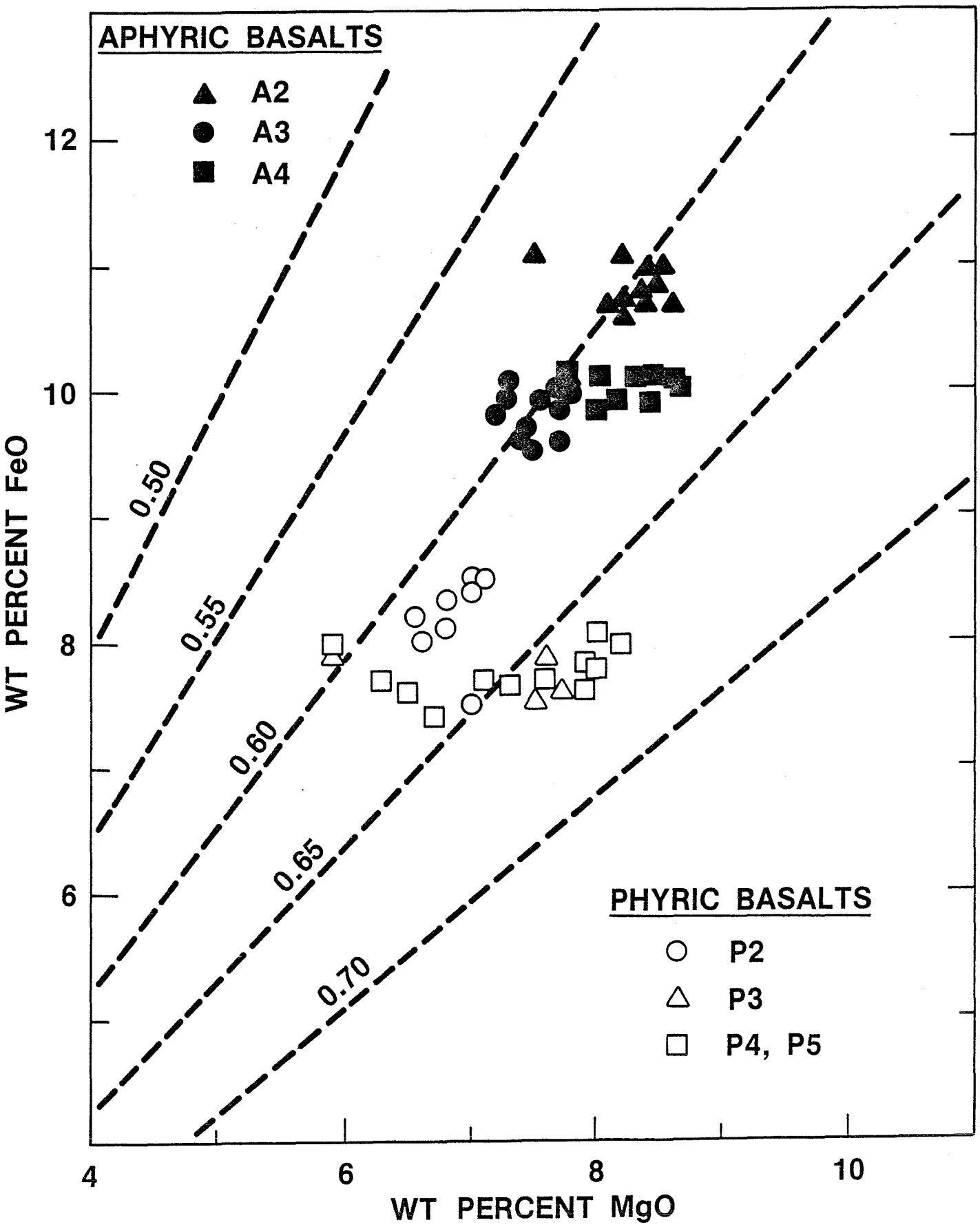

NASA-S-77-11445

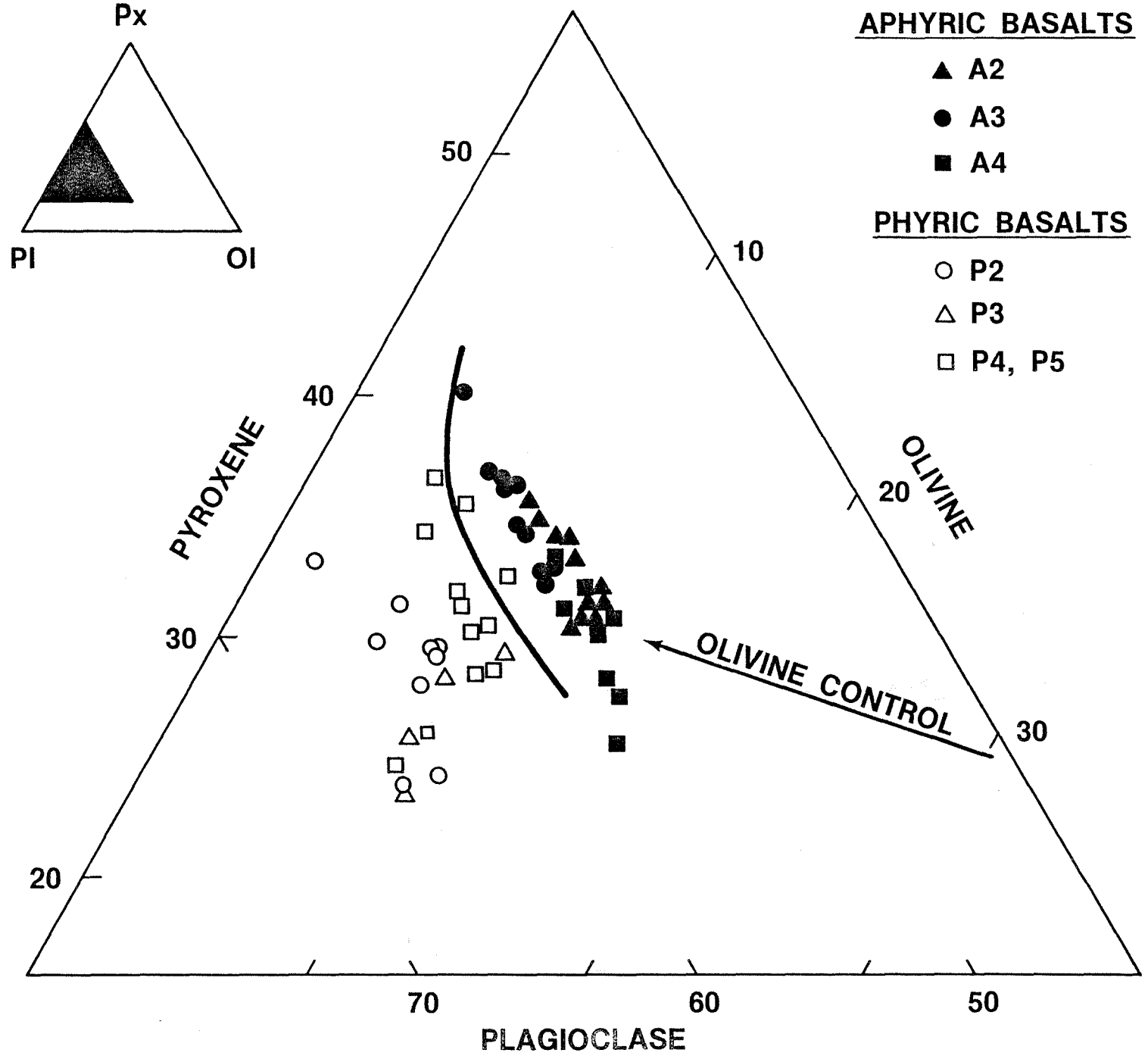

NASA-S-77-11449

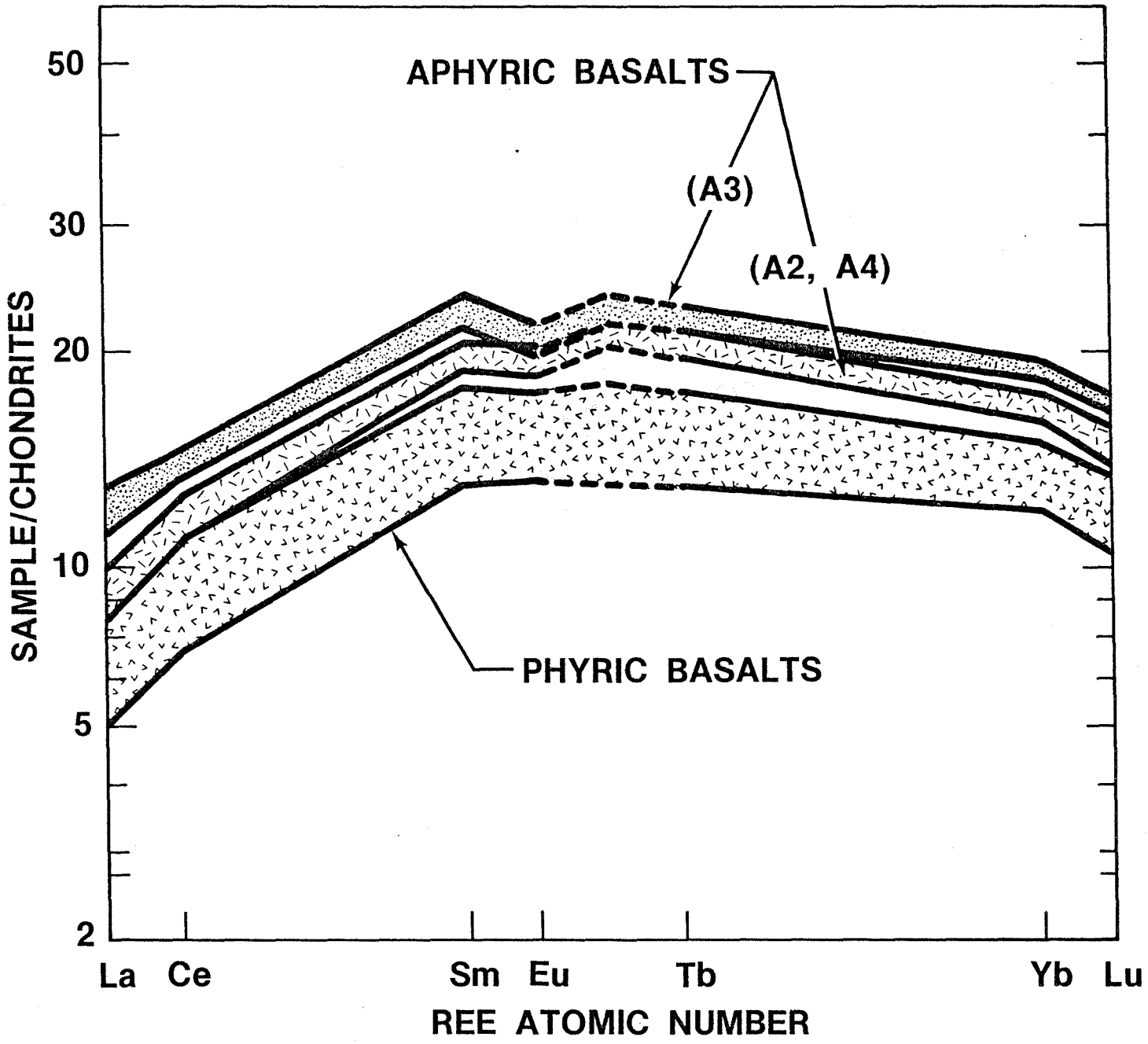

NASA-S-77-11447

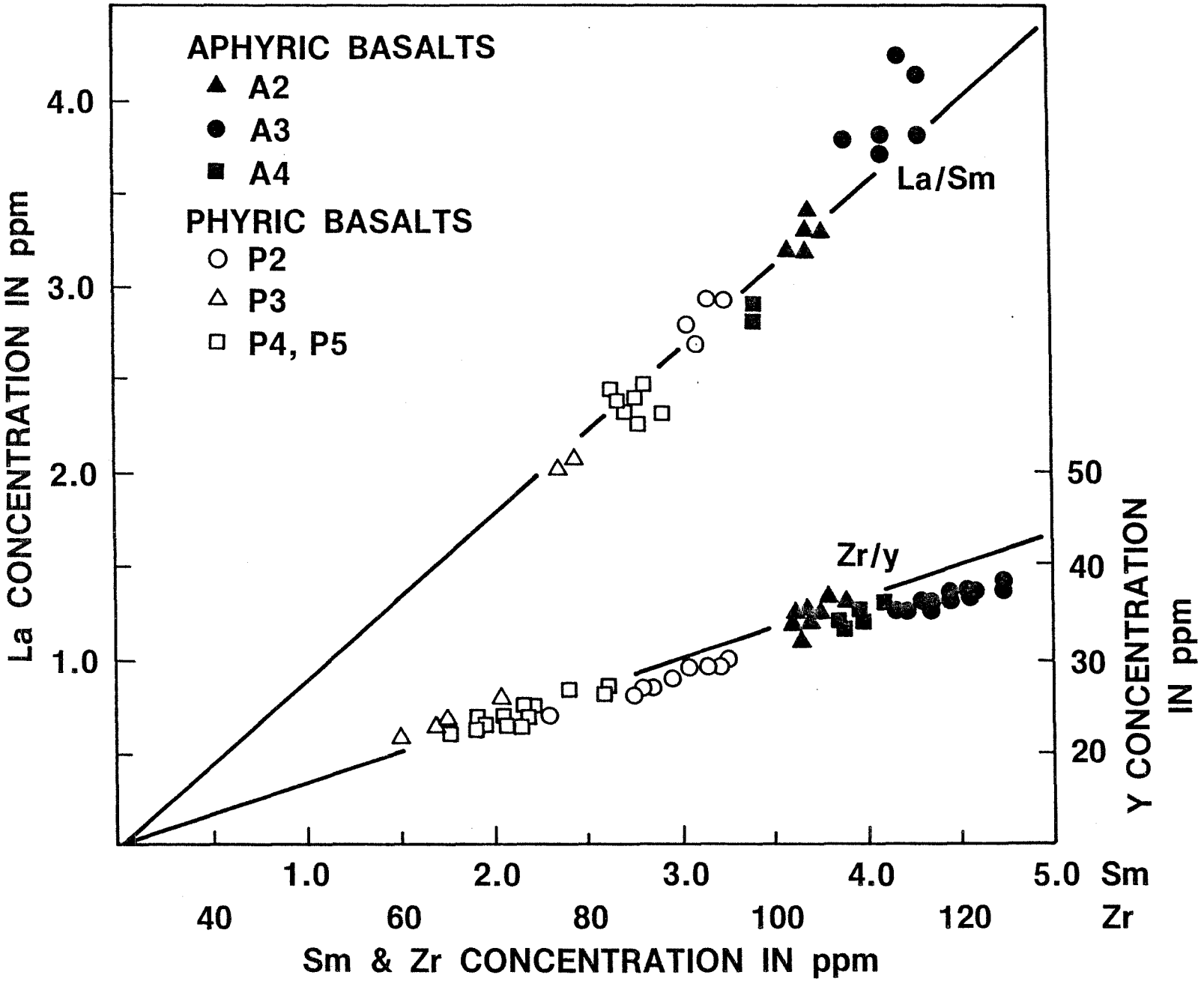

Table 1.- Chemical composition of basalts from Site 395

Hole	395	395	395	395	395	395	395	395	395A	395A	395A
Core-Section	11-1	11-1	11-2	15-2	16-2	16-3	18-2	19-1	4-1	5-1	6-1
cm interval	42-44	136-138	100-105	68-72	63-66	3-8	43-46	57-62	66-69	6-10	130-134
JSC No.	109	110	111	112	113	114	115	116	117	118	119
Depth m	93	94	95	133	142	143	161	170	98	106	117
Basalt type	A_2*	A_2*	A_2*	A_2*	A_2*	A_2*	P_1*	P_2*	A_3	A_2	A_2
SiO_2	49.4	49.3	48.5	49.3	49.6	48.9	48.8	49.7	49.5	49.2	48.7
TiO_2	1.62	1.61	1.58	1.60	1.66	1.60	1.14	1.29	1.70	1.63	1.60
Al_2O_3	15.09	14.84	14.79	14.68	15.15	14.69	16.67	18.48	15.18	15.11	14.74
Fe_2O_3	1.28	1.36	1.81	2.61	4.62	2.20	2.90	3.23	2.86	3.95	4.30
FeO	9.83	9.73	9.06	8.33	6.94	8.87	5.90	4.45	7.44	6.04	6.82
MnO	0.20	0.19	0.17	0.18	0.19	0.18	0.15	0.12	0.17	0.17	0.18
MgO	8.51	8.45	8.56	8.40	8.17	8.47	8.07	5.99	7.69	7.74	8.08
CaO	10.41	10.34	10.18	10.17	10.43	10.25	12.24	12.10	11.17	11.03	10.11
Na_2O	2.80	2.92	2.82	2.89	2.82	2.87	2.34	2.68	2.74	2.79	2.97
K_2O	0.11	0.10	0.14	0.14	0.16	0.17	0.13	0.11	0.28	0.26	0.22
P_2O_5	0.13	0.11	0.12	0.13	0.16	0.12	0.09	0.10	0.15	0.17	0.12
S	0.11	0.11	0.11	0.12	0.10	0.14	0.05	0.03	0.07	0.05	0.07
Total H_2O	0.55	0.43	1.56	1.42	0.91	1.53	0.89	1.97	1.08	1.51	2.48
Total	100.04	99.50	99.37	99.94	100.94	99.94	99.38	100.27	100.04	99.64	100.45
Total Fe as FeO	10.98	10.95	10.69	10.68	11.10	10.85	8.51	7.36	10.01	9.60	10.69
Mg-value	0.605	0.605	0.613	0.609	0.593	0.607	0.653	0.617	0.603	0.615	0.599
O. R.	0.117	0.124	0.169	0.244	0.416	0.203	0.341	0.439	0.286	0.411	0.402
Trace elements (ppm)											
Rb	1.2	0.9	1.7	1.1	1.1	1.1	1.5	1.2	2.6	3.3	3.0
Sr	115	112	116	116	115	118	110	158	131	129	118
Y	35	35	34	35	37	36	26	26	36	35	34
Zr	105	105	102	106	106	108	71	85	119	113	104
Nb	2.4	1.9	1.9	1.7	1.8	2.1	1.1	2.0	2.3	1.9	2.0
Ni											

Table 1.- continued

Hole	395A	395A	395A	395A	395A	395A	395A	395A	395A	395A	395A
Core-Section	8-1	9-1	9-2	10-1	13-1	14-2	14-3	15-1	15-4	15-4	15-4
cm interval	70-73	73-79	100-104	144-146	142-147	140-147	29-34	75-81	10-15	10-15	99-107
JSC No.	120	121	122	123	124	125	126	127	128(1)	128(2)	129
Depth m	126	135	137	145	174	185	186	192	196	196	197
Basalt type	A_2	A_2	A_2	A_2	P_2	P_2	P_2	P_2	P_2	P_2	P_2
SiO_2	48.7	48.5	48.9	48.8	49.2	49.1	49.7	49.0	49.0	49.5	48.3
TiO_2	1.66	1.60	1.63	1.60	1.37	1.34	1.33	1.35	1.36	1.35	1.30
Al_2O_3	15.40	14.69	14.92	14.90	17.34	17.93	18.13	17.51	17.65	17.57	18.01
Fe_2O_3	2.56	2.84	2.67	1.97	2.52	1.57	2.40	2.69	1.40	(1.40)	2.34
FeO	8.81	8.03	8.20	8.96	5.96	6.94	5.86	5.97	7.25	7.25	5.96
MnO	0.20	0.20	0.19	0.19	0.15	0.13	0.14	0.13	0.13	0.14	0.15
MgO	7.60	8.21	8.15	8.40	6.55	6.81	6.58	6.97	7.07	7.03	6.82
CaO	10.46	10.17	10.29	10.23	11.54	11.73	11.74	11.54	11.58	11.57	11.51
Na_2O	2.90	2.93	3.01	2.90	2.83	2.80	2.85	2.76	2.71	(2.71)	2.87
K_2O	0.18	0.16	0.15	0.14	0.11	0.09	0.07	0.11	0.11	0.11	0.08
P_2O_5	0.17	0.12	0.13	0.12	0.10	0.10	0.12	0.11	0.12	0.12	0.09
S	0.10	0.14	0.14	0.13	0.09	0.10	0.12	0.12	0.11	0.11	0.08
Total H_2O	1.62	1.93	1.25	1.41	1.94	1.48	1.46	1.63	1.71	—	1.65
Total	100.33	99.56	99.61	99.79	99.66	100.12	100.49	99.87	100.21		99.20
Total Fe as FeO	11.11	10.59	10.60	10.73	8.23	8.35	8.02	8.39	8.51	8.52	8.07
Mg'-value	0.575	0.606	0.604	0.608	0.612	0.618	0.619	0.622	0.622	0.620	0.626
O. R.	0.230	0.269	0.252	0.184	0.306	0.188	0.299	0.321	0.165	——	0.343
Trace elements (ppm)											
Rb	1.6	1.5	1.3	1.3	1.1	0.9	0.5	1.0	1.3	1.0	0.5
Sr	119	118	114	115	153	152	152	155	156	152	154
Y	35	35	36	32	29	27	27	30	29	29	28
Zr	104	103	106	103	94	87	86	95	91	93	89
Nb	2.0	1.7	1.6	2.1	1.7	1.2	1.9	1.4	1.4	1.8	1.7
Ni											

Table 1.- continued

Hole	395A	395A	395A	395A	395A	395A	395A	395A	395A	395A	395A
Core-Section	15-5	17-1	19-1	21-1	23-1	24-2	25-1	26-2	27-2	38-1	29-1
cm interval	16-20	46-55	132-136	87-90	51-55	69-72	96-100	125-129	111-116	105-112	125-131
JSC No.	130	131	132	133	134	135	136	137	138	139	141
Depth m	198	211	231	242	261	272	280	292	301	309	317
Basalt type	P_2	P_3	P_3	P_3	P_4	P_4	P_4	P_4	P_4	P_5	P_5
SiO_2	48.9	48.9	49.1	49.8	49.2	49.1	49.3	38.9	49.6	48.8	49.8
TiO_2	1.14	1.09	1.08	1.03	1.12	1.15	1.14	1.25	1.14	1.19	1.14
Al_2O_3	19.16	18.05	16.85	17.73	18.51	17.26	17.10	18.85	17.13	19.09	17.07
Fe_2O_3	1.47	3.70	3.42	2.58	3.76	2.80	2.58	3.41	1.94	.307	2.65
FeO	6.19	4.78	4.80	5.23	4.24	5.11	5.28	4.85	6.03	4.97	5.73
MnO	0.13	0.15	0.13	0.14	0.14	0.15	0.14	0.17	0.15	0.15	0.15
MgO	6.96	6.66	7.61	7.53	6.51	7.90	7.67	5.87	8.03	6.33	8.00
CaO	11.83	12.83	12.19	12.49	12.59	12.17	11.99	12.27	12.08	12.22	12.04
Na_2O	2.75	2.50	2.31	2.39	2.75	2.65	2.62	2.84	2.64	2.78	2.59
K_2O	0.07	0.12	0.13	0.15	0.15	0.13	0.14	0.16	0.15	0.15	0.13
P_2O_5	0.09	0.09	0.08	0.10	0.12	0.09	0.11	0.13	0.10	0.11	0.10
S	0.09	0.01	0.01	0.03	0.01	0.00	0.01	0.02	0.02	0.02	0.02
Total H_2O	1.63	1.19	1.94	1.68	1.01	0.88	1.54	1.26	0.71	0.97	0.83
Total	100.41	100.08	99.67	100.91	100.10	99.42	99.58	99.96	99.69	99.87	99.41
Total Fe as FeO	7.51	8.11	7.88	7.55	7.62	7.63	7.60	7.92	7.78	7.73	8.11
Mg-value	0.647	0.619	0.657	0.664	0.629	0.672	0.667	0.595	0.671	0.619	0.661
O. R.	0.196	0.456	0.434	0.342	0.493	0.367	0.339	0.431	0.249	0.397	0.327
Trace elements (ppm)											
Rb	0.6	1.9	2.1	1.7	1.4	1.5	2.3	2.5	2.1	2.7	2.0
Sr	153	119	110	112	138	131	133	165	129	159	132
Y	24	24	23	22	24	25	24	26	25	27	25
Zr	76	65	64	60	68	72	73	82	73	82	74
Nb	0.7	0.9	1.2	1.5	1.3	1.5	0.9	1.3	1.0	1.1	1.3
Ni											

Table 1.- continued

Hole	395A	395A	395A	395A	395A	395A	395A	395A	395A	395A	395A
Core-Section	31-1	33-1	34-1	35-1	36-1	38-1	41-1	46-1	49-1	50-2	51-3
cm interval	96-107	142-148	140-143	26-32	46-50	142-148	107-111	61-64	26-31	143-147	78-82
JSC No.	142	143	144	145	146	147	148	149	150	151	152
Depth m	337	355	364	373	383	393	428	476	504	516	526
Basalt type	P_5	P_5	A_3	A_3	A_3	A_3	A_3	A_3	A_3	A_3	A_4
SiO_2	49.8	48.9	49.5	49.3	48.9	48.6	49.7	49.3	49.5	48.8	48.8
TiO_2	1.10	1.14	1.69	1.67	1.67	1.65	1.70	1.75	1.74	1.72	1.70
Al_2O_3	18.62	17.55	15.32	1.501	15.13	14.61	15.30	15.10	15.13	15.07	14.93
Fe_2O_3	3.28	4.08	2.98	4.50	4.10	4.15	2.90	3.90	3.14	3.97	3.52
FeO	4.49	4.00	7.24	5.66	5.80	5.83	7.28	6.29	7.24	6.38	6.67
MnO	0.12	0.14	0.19	0.16	0.19	0.17	0.17	0.19	0.19	0.16	0.18
MgO	6.69	7.11	7.61	7.45	7.48	7.40	7.28	7.21	7.29	7.67	7.69
CaO	12.17	11.85	11.21	10.95	11.09	10.83	11.14	11.10	11.19	11.02	10.87
Na_2O	2.89	2.73	2.80	2.88	2.93	2.89	2.82	2.90	2.84	2.85	2.88
K_2O	0.18	0.18	0.22	0.32	0.26	0.22	0.22	0.31	0.18	0.22	0.26
P_2O_5	0.08	0.11	0.17	0.13	0.14	0.14	0.15	0.17	0.17	0.16	0.15
S	0.01	0.01	0.09	0.03	0.02	0.004	0.08	0.02	0.09	0.05	0.07
Total H_2O	1.77	1.86	1.33	1.95	2.28	2.00	1.11	1.26	1.30	1.76	1.77
Total	101.23	99.66	100.32	100.03	100.03	98.53	99.85	99.50	99.97	99.84	99.51
Total Fe as FeO	7.44	7.67	9.92	9.71	9.49	9.56	9.89	9.80	10.07	9.95	9.84
Mg'-value	0.614	0.647	0.603	0.603	0.609	0.605	0.593	0.593	0.589	0.604	0.607
O. R.	0.440	0.532	0.300	0.463	0.432	0.434	0.293	0.227	0.312	0.399	0.358
Trace elements (ppm)											
Rb	2.6	2.5	1.0	4.7	3.3	2.3	0.7	4.5	1.5	2.8	2.3
Sr	175	151	127	133	130	134	129	132	131	130	129
Y	23	23	36	35	36	35	36	37	37	37	37
Zr	71	73	116	117	117	114	117	125	121	121	122
Nb	0.8	1.0	2.4	2.0	1.9	2.0	2.1	2.2	2.5	1.9	2.1
Ni											

Table 1.- continued

Hole	395A	395A	395A	395A	395A	395A	395A	395A	395A	395A	395A
Core-Section	52-2	56-3	57-1	59-1	60-1	60-3	61-1	62-1	63-1	63-4	64-1
cm interval	75-80	62-65	40-43	67-70	66-70	33-37	142-150	10-15	42-47	86-93	29-37
JSC No.	153	154	155	156	157	158	159	160	161	162	163
Depth m	534	565	570	590	599	602	608	617	619	624	626
Basalt type	A_3	A_3	A_4	A_4	A_4	A_4	P_4'	P_4'	P_4'	P_4'	P_4'
SiO_2	50.3	49.4	48.8	48.3	48.4	47.2	49.2	49.3	49.6	48.5	49.1
TiO_2	1.73	1.75	1.57	1.58	1.59	1.55	1.21	1.09	1.12	1.06	1.06
Al_2O_3	15.22	14.99	14.93	14.93	15.12	15.09	16.05	17.15	16.47	17.19	17.21
Fe_2O_3	2.94	3.21	2.32	2.69	3.21	5.02	3.81	2.10	2.68	3.92	3.27
FeO	7.37	7.12	8.02	7.65	6.94	5.36	4.92	5.93	5.56	4.16	4.71
MnO	0.19	0.18	0.19	0.16	0.19	0.18	0.15	0.16	0.17	0.15	0.16
MgO	7.34	7.82	8.62	8.45	8.01	8.40	7.84	7.93	8.18	7.56	7.31
CaO	11.10	10.82	10.55	10.71	10.77	10.60	11.71	11.63	11.59	11.77	12.45
Na_2O	2.76	2.80	2.80	2.83	2.85	2.77	2.72	2.70	2.54	2.64	4.21
K_2O	0.19	0.19	0.15	0.13	0.14	0.16	0.16	0.08	0.09	0.12	0.10
P_2O_5	0.16	0.18	0.15	0.13	0.12	0.13	0.10	0.08	0.09	0.09	0.08
S	0.11	0.07	0.09	0.05	0.07	0.01	0.01	0.11	0.05	0.00	0.02
Total H_2O	1.38	1.44	1.50	1.84	1.95	2.17	1.66	1.75	1.78	2.75	1.31
Total	100.75	100.02	99.51	99.42	99.36	98.61	99.55	100.02	99.92	99.90	100.87
Total Fe as FeO	10.02	10.01	10.11	10.07	9.83	9.88	8.35	7.82	7.97	7.69	7.65
Mg-value	0.592	0.607	0.628	0.624	0.617	0.627	0.650	0.668	0.670	0.661	0.654
O. R.	0.293	0.321	0.229	0.267	0.326	0.508	0.456	0.269	0.336	0.510	0.427
Trace elements (ppm)											
Rb	1.0	1.2	0.9	0.6	0.9	2.2	3.9	0.8	1.0	4.0	1.7
Sr	128	127	121	125	125	117	128	122	123	130	136
Y	37	38	34	34	35	34	27	23	24	22	23
Zr	119	125	107	109	109	103	78	69	71	65	68
Nb	2.8	2.7	2.4	2.4	1.8	2.3	0.6	1.1	0.3	0.8	0.9
Ni											

Table 1.- concluded

Hole	395A	395A	395A	395A	395A
Core-Section	64-4	64-cc	66-1	66-3	67-cc
cm interval	130-135	17-21	36-41	12-16	130-135
JSC No.	164	165	166	167	168
Depth m	631	632	645	648	657
Basalt type	A_4	A_4	A_4	A_4	A_5
SiO_2	47.1	48.8	48.1	47.7	48.2
TiO_2	1.59	1.56	1.61	1.59	1.57
Al_2O_3	15.00	15.07	15.02	14.76	14.87
Fe_2O_3	5.07	3.90	3.84	4.71	2.48
FeO	5.49	6.36	6.63	5.87	7.86
MnO	0.19	0.17	0.18	0.21	0.18
MgO	7.72	8.15	8.32	7.99	8.57
CaO	10.67	10.77	10.77	10.67	10.85
Na_2O	2.96	2.76	2.77	2.96	2.69
K_2O	0.15	0.17	0.12	0.18	0.22
P_2O_5	0.13	0.13	0.14	0.14	0.15
S	0.00	0.08	0.05	0.00	0.08
Total H_2O	3.08	2.03	2.28	2.62	1.96
Total	99.13	99.94	99.83	99.37	99.72
Total Fe as FeO	10.05	9.87	10.09	10.11	10.09
Mg-value	0.603	0.621	0.620	0.610	0.627
O. R.	0.505	0.395	0.381	0.466	0.246
Trace elements (ppm)					
Rb	2.3	1.9	1.3	3.8	0.9
Sr	126	132	127	126	122
Y	35	33	36	35	34
Zr	108	107	112	109	107
Nb	2.7	1.8	2.0	2.5	1.4
Ni					

Table 2.- Chemical composition of basalts from Site 396

Hole	396	396	396	396	396	396	396	396
Core-Section	14-6	15-1	16-1	18-3	22-2	23-1	24-2	25-1
cm interval	94-100	110-115	97-101	147-150	120-128	58-61	49-54	134-139
JSC No.	174	173	176	175	171	172	169	170
Depth m	120	127	137	159	193	201	211	221
Basalt type								
SiO_2	49.00	49.30	48.79	49.27	48.99	49.17	49.81	49.30
TiO_2	1.51	1.27	1.26	1.29	1.23	1.25	1.30	1.29
Al_2O_3	16.85	16.95	16.86	16.30	16.69	17.29	16.52	16.21
Fe_2O_3	4.23	1.39	3.64	3.85	3.65	4.33	3.92	4.43
FeO	5.19	7.15	4.90	4.72	4.68	4.19	5.02	4.68
MnO	0.18	0.17	0.15	0.14	0.14	0.13	0.17	0.17
MgO	6.05	7.48	8.03	7.66	7.60	6.42	7.21	6.86
CaO	11.59	11.80	11.85	11.48	11.66	12.07	11.76	11.69
Na_2O	2.79	2.66	2.87	2.75	2.79	2.77	2.72	2.68
K_2O	0.26	0.20	0.21	0.23	0.24	0.20	0.23	0.25
P_2O_5	0.13	0.09	0.08	0.08	0.09	0.09	0.09	0.15
S	0.06	0.05	0.05	0.02	0.02	0.02	0.01	0.03
Total H_2O	1.73	1.49	1.52	2.28	2.47	2.86	2.10	2.52
Total	99.57	100.00	100.21	100.70	100.24	100.79	100.86	100.26
Total Fe as FeO	9.00	8.40	8.17	8.18	7.96	8.09	8.55	8.68
Mg'-value	0.571	0.638	0.661	0.650	0.654	0.611	0.626	0.610
O.R.	0.470	0.165	0.445	0.471	0.459	0.535	0.459	0.510
Trace elements (ppm)								
Rb	2.5	1.0	2.5	2.7	3.3	2.9	3.5	
Sr	152	149	145	160	145	152	127	
Y	33	26	27	28	26	27	28	
Zr	105	84	85	87	83	79	83	
Nb	2.3	2.1	1.4	1.6	2.0	1.1	1.4	
Ni								

Table 3.- Trace Element Abundances (ppm) in Selected DSDP Leg 45 Samples

Hole	395	395	395	395A	395A	395A	395A	395A	395A	395A	395A	395A	395A
Core-Section	11-1	11-2	19-1	4-1	8-1	10-1	14-2	15-4	15-4	15-5	15-5	19-1	21-1
cm interval	42-44	100-105	57-62	66-69	70-73	144-146	140-147	10-15	16-20	16-20	16-20	132-136	87-90
J.S.C. No.	109	111	116	117	120	123	125	128(1)	128(2)	130	130	132	133
Depth, m	95	101	173	99	129	153	186	199	199	201	201	231	244
Basalt type	A_2	A_2	P_2	A_3	A_2	A_2	P_2	P_2	P_2	P_2	P_2	P_3	P_3
Sc	36.6	36.0	29.8	38.4	37.9	37.1	31.1	31.5	32.6	28.2	29.0	32.5	32.4
Cr	290	290	252	320	300	300	220	290	250	260	300	377	380
Ni	120	190	110	140	140	150	87	83	90	100	70	110	130
La	2.91	2.79	2.71	3.77	3.18	3.31	2.93	2.79	2.95	2.42	2.40	2.02	2.07
Ce	9.6	9.7	9.3	12.2	11.1	9.8	9.5	9.2	9.7	8.0	7.8	6.7	6.8
Sm	3.38	3.41	3.09	3.91	3.72	3.68	3.20	3.05	3.26	2.66	2.68	2.38	2.45
Eu	1.33	1.27	1.06	1.40	1.39	1.34	1.17	1.16	1.20	1.01	1.03	0.91	0.93
Tb	0.92	0.92	0.76	1.0	0.95	0.95	0.82	0.71	0.76	0.64	0.69	0.66	0.62
Yb	3.3	3.2	2.8	3.5	3.6	3.7	3.0	2.7	2.8	2.4	2.4	2.4	2.4
Lu	0.50	0.47	0.42	0.53	0.52	0.56	0.45	0.42	0.46	0.37	0.36	0.36	0.37
Hf	3.0	2.7	2.3	3.0	3.0	2.9	2.4	2.4	2.6	2.1	1.9	1.9	1.9

Hole	395A	395A	395A	395A	395A	395A	395A	395A	395A	395A	395A	395A	395A
Core-Section	25-1	27-2	31-1	34-1	41-1	49-1	52-2	56-3	57-1	61-1	63-4	66-1	67-cc
cm interval	96-100	111-116	96-107	140-143	107-111	26-31	75-80	62-65	40-43	142-150	86-93	36-41	130-135
J.S.C. No.	136	138	142	144	148	150	153	154	155	159	162	166	168
Depth, m	285	306	339	372	433	504	539	567	573	609	626	645	660
Basalt type	P_4	P_4	P_5	A_3	A_3	A_3	A_3	A_3	A_4	P_4	P_4	A_4	A_4
Sc	33.8	33.5	32.3	38.5	38.7	38.8	37.8	38.3	36.7	35.6	30.6	36.7	36.6
Cr	340	340	310	280	290	290	280	260	340	320	380	320	330
Ni	150	130	140	110	100	40	120	120	170	110	140	140	140
La	2.41	2.33	2.48	3.82	3.70	4.14	3.81	4.24	3.34	2.24	2.30	3.18	3.37
Ce	8.1	7.2	8.1	11.7	12.3	12.5	12.1	12.6	10.4	8.2	8.4	10.3	10.6
Sm	2.77	2.72	2.82	4.10	4.09	4.28	4.33	4.20	3.67	2.81	2.93	3.56	3.67
Eu	1.06	1.04	1.06	1.43	1.47	1.45	1.36	1.51	1.34	1.08	1.08	1.39	1.33
Tb	0.72	0.60	0.67	0.99	1.05	1.09	1.02	1.06	0.93	0.72	0.72	0.99	0.94
Yb	2.5	2.7	2.7	3.7	3.6	3.8	3.9	3.9	3.3	2.5	2.6	3.2	3.6
Lu	0.40	0.40	0.41	0.56	0.55	0.56	0.59	0.58	0.53	0.38	0.43	0.47	0.50
Hf	2.3	2.2	2.2	3.3	3.3	3.2	3.2	3.2	3.1	2.2	2.4	2.8	3.3

Table 4: Average compositions of Leg 45 Basalt Types

	APHYRIC BASALTS			PHYRIC BASALTS				
	A2	A3	A4	P2	P3	P4	P4 sill	P5
Major Elements (wt. %)								
SiO_2	48.96	49.28	48.07	49.16	49.27	49.22	49.15	49.13
TiO_2	1.61	1.71	1.58	1.31	1.07	1.16	1.11	1.14
Al_2O_3	14.90	15.07	14.98	17.98	17.54	17.77	16.81	18.08
FeO*	10.81	9.84	10.01	8.11	7.85	7.71	7.90	7.74
MnO	0.19	0.18	0.18	0.14	0.14	0.15	0.16	0.14
MgO	8.27	7.48	8.36	6.75	7.27	7.20	7.76	7.03
CaO	10.28	11.03	10.71	11.68	12.50	12.22	11.83	12.07
Na_2O	2.89	2.85	2.82	2.78	2.40	2.70	2.65	2.75
K_2O	0.15	0.23	0.16	0.10	0.13	0.15	0.11	0.16
P_2O_5	0.13	0.16	0.13	0.11	0.09	0.11	0.09	0.10
S	0.11	0.06	0.04	0.09	0.02	0.01	0.04	0.02
Mg'-value	0.602	0.601	0.623	0.622	0.647	0.649	0.661	0.643
Trace Elements (ppm)								
Rb	1.4	2.3	1.6	0.9	1.9	2.0	2.3	2.5
Sr	116	130	125	154	114	139	129	154
Y	34.9	36.5	34.4	27.7	23.0	24.8	23.8	24.5
Zr	105	119	108	88	63	74	70	75
Nb	1.9	2.2	2.1	1.5	1.2	1.2	0.7	1.1
La	3.05	3.94	3.30	2.70	2.05	2.37	2.27	2.48
Ce	10.1	12.2	10.4	8.9	6.7	7.7	8.3	8.1
Sm	3.55	4.20	3.63	2.99	2.42	2.75	2.87	2.82
Eu	1.33	1.44	1.35	1.11	0.92	1.05	1.08	1.06
Tb	0.94	1.04	0.95	0.73	0.64	0.76	0.72	0.67
Yb	3.5	3.8	3.4	2.7	2.4	2.6	2.5	2.7
Lu	0.51	0.57	0.50	0.41	0.36	0.40	0.40	0.41
Hf	2.9	3.2	3.1	2.3	1.9	2.3	2.3	2.2
Sc	36.9	38.4	36.7	30.4	32.5	33.7	33.1	32.3
Cr	295	280	330	262	379	340	350	310
Ni	150	98	150	90	120	140	125	140
La/Sm	0.86	0.94	0.91	0.90	0.85	0.86	0.79	0.88
La/Yb	0.87	1.04	0.97	1.00	0.85	0.91	0.91	0.92
Sm/Eu	2.67	2.92	2.69	2.69	2.63	2.62	2.66	2.66
Sr/Zr	1.10	1.09	1.16	1.75	1.81	1.88	1.84	2.05
Zr/Nb	55	54	51	59	53	62	100	68
Zr/Y	3.01	3.26	3.14	3.2	2.7	3.0	2.9	3.1
Ti/Zr	92	86	88	89	102	94	95	91
Zr/Hf	36	37	35	38	33	32	30	34